

Mapping plasmonic near-field profiles and interferences by surface-enhanced Raman scattering

Du, Luping; Lei, Dang Yuan; Yuan, Guanghui; Fang, Hui; Zhang, Xi; Wang, Qian; Tang, Dingyuan; Min, Changjun; Maier, Stefan A.; Yuan, Xiaocong

2013

Du, L., Lei, D. Y., Yuan, G., Fang, H., Zhang, X., Wang, Q., et al. (2013). Mapping plasmonic near-field profiles and interferences by surface-enhanced Raman scattering. *Scientific reports*, 3, 1-6.

<https://hdl.handle.net/10356/101424>

<https://doi.org/10.1038/srep03064>

© 2013 The Authors. This paper was published in *Scientific Reports* and is made available as an electronic reprint (preprint) with permission of the authors. The paper can be found at the following official DOI: [<http://dx.doi.org/10.1038/srep03064>]. One print or electronic copy may be made for personal use only. Systematic or multiple reproduction, distribution to multiple locations via electronic or other means, duplication of any material in this paper for a fee or for commercial purposes, or modification of the content of the paper is prohibited and is subject to penalties under law.

Downloaded on 23 Sep 2021 08:26:33 SGT



OPEN

Mapping plasmonic near-field profiles and interferences by surface-enhanced Raman scattering

SUBJECT AREAS:

MICROSCOPY

NANOPHOTONICS AND
PLASMONICS

Received

22 July 2013

Accepted

7 October 2013

Published

29 October 2013

Correspondence and requests for materials should be addressed to X.C.Y. (xcyuan@szu.edu.cn)

Luping Du¹, Dang Yuan Lei², Guanghui Yuan¹, Hui Fang³, Xi Zhang¹, Qian Wang¹, Dingyuan Tang¹, Changjun Min³, Stefan A. Maier⁴ & Xiaocong Yuan⁵

¹School of Electrical & Electronic Engineering, Nanyang Technological University, Nanyang Avenue 639798, Singapore, ²Department of Applied Physics, The Hong Kong Polytechnic University, Hong Kong, China, ³Institute of Modern Optics, Key Laboratory of Optical Information Science & Technology, Ministry of Education of China, Nankai University, Tianjin 300071, China, ⁴The Blackett Laboratory, Department of Physics, Imperial College London, London SW7 2AZ, UK, ⁵Institute of Micro & Nano Optics, College of Optoelectronic Engineering, Shenzhen University, Shenzhen, 518060, China.

Mapping near-field profiles and dynamics of surface plasmon polaritons is crucial for understanding their fundamental optical properties and designing miniaturized photonic devices. This requires a spatial resolution on the sub-wavelength scale because the effective polariton wavelength is shorter than free-space excitation wavelengths. Here by combining total internal reflection excitation with surface-enhanced Raman scattering imaging, we mapped at the sub-wavelength scale the spatial distribution of the dominant perpendicular component of surface plasmon fields in a metal nanoparticle-film system through spectrally selective and polarization-resolved excitation of the vertical gap mode. The lateral field-extension at the junction, which is determined by the gap-mode volume, is small enough to distinguish a spot size $\sim 0.355\lambda_0$ generated by a focused radially polarized beam with high reproducibility. The same excitation and imaging schemes are also used to trace near-field nano-focusing and interferences of surface plasmon polaritons created by a variety of plasmon lenses.

Surface plasmon polaritons (SPPs) are light-induced charge-density waves propagating along the interface between a dielectric and a conductor, evanescently confined in the perpendicular direction¹ with large near-field enhancement. SPPs excitations are highly sensitive to perturbations in their vicinity, resulting in a strong environment-dependent optical response. These unique features make SPPs extremely versatile in a broad range of applications, including ultrahigh-sensitivity spectroscopy² and biosensing³, super-resolution imaging⁴, sub-diffraction-limited nanolithography⁵ and miniaturized photonic circuits⁶.

Being able to map the field distribution of SPPs is crucial for understanding their fundamental properties and facilitating applications. The conventional method of choice is scanning near-field optical microscopy (SNOM)⁷, since it fits very well the requirements of near-field detection with high lateral-resolution. In an aperture-type SNOM system^{8–13}, a bare tapered or metal-coated fiber is dipped into the surface plasmon evanescent field to couple some of its energy into propagating waves. The coupling efficiency of in-plane and perpendicular electric-field components of SPPs to the fiber depends strongly on the geometry of the tip aperture^{14,15}. Previous experiments have indicated a high collection efficiency of the in-plane field^{9,16}, but unfortunately this is a subordinated component that accounts for less than 10% of the field strength for SPPs of wave vectors close to the light wave vector. This jeopardizes the goal of capturing the whole scenario of SPPs as the dominant perpendicular component is not directly accessed for characterization. In contrast, a scattering-type SNOM uses an aperture-free tip with apex dimension much smaller than the wavelength of incident light, similar to that used in AFM and STM systems⁷. As the probe tip is located in close proximity to a metal surface, Rayleigh scattering of the evanescent fields of SPPs occurs and the resulting scattering radiation is collected with a lens-based system in the far-field regime. To obtain a reliable near-field image, removing background signals (including the incident light and scattering radiation induced by other scatterers rather than the probe tip) is a critical issue, which usually involves the use of a lock-in amplifier to pick up the modulated scattering signal at the frequency of cantilever oscillations^{17–19}.

Other state-of-the-art techniques that can potentially be used to characterize the propagation dynamics of SPPs include leakage radiation microscopy²⁰ and fluorescence imaging²¹. Although these techniques can perform



real-time imaging of the total intensity of SPPs, the optical diffraction-limit restricts their resolution, thus hindering a detailed analysis in many situations such as near-field nano-focusing and interference patterns with high spatial frequencies. In addition, both techniques fail to capture or distinguish the dominant component of the total surface plasmon fields. Therefore, development of an accurate, faithful and easy-to-use mapping tool for characterizing SPPs, especially for collecting the strongly-dominant perpendicular components in a general class of plasmonic systems, is critically needed for extending our understanding of the fundamental properties of SPPs and facilitating the development of plasmonic devices.

As a variant of the scattering-type SNOM, we report here a novel near-field characterization scheme based on the combination of total internal reflection excitation and surface-enhanced Raman scattering (SERS) imaging. With the proposed scheme, we show the mapping of the perpendicular component of SPPs in a metal nanoparticle-film system at the subwavelength scale. The electromagnetic field associated with plasmon hybridized gap modes is strongly confined within the particle-film junction and used to enhance the Raman scattering of molecules within the gap. Polarization-resolved excitations of the gap modes and subsequent SERS imaging further confirm the efficient capture of the perpendicular field component of SPPs. As demonstrations, we first examine the SPP patterns produced by focusing a cylindrical beam into a Kretschmann-type structure of a thin metal film deposited on a glass plate. For a radially polarized cylindrical beam²², the detected SPP pattern shows a center spot of $0.355\lambda_0$, which agrees well with theory. Following the same methodology, we visualize directly nano-focusing and interferences of surface plasmon waves created by a particular class of plasmonic near-field lenses, further demonstrating the universal use of the developed near-field imaging method for more general evanescent wave characterizations at subwavelength scales.

Results

Principle of surface plasmon characterization by SERS imaging.

Near-field coupling between propagating surface plasmons on the metal film and localized surface plasmons of the nanoparticle in a metal particle-film junction system offers a unique opportunity to extract the perpendicular component of the former plasmon. For example, considering the surface plasmon fields produced from focusing a radially polarized cylindrical beam (see Fig. 1a), where a plasmonic standing-wave interference pattern is formed on the metal film, free electrons and virtual ions will concentrate alternatively at the standing-wave nodes (see Fig. 1b). Upon introducing a sphere-shaped nanoparticle, a vertically-oriented gap mode is excited at the nodes by the perpendicular electric-field of SPPs while a laterally aligned gap mode is formed at the anti-nodes where the in-plane electric-field dominates (see Fig. 1b). The different schemes for nanosphere-film interaction result in an energy splitting between the vertical and lateral modes, as we will show later.

The nanoparticle-film interaction strength is governed by the Coulomb interaction between the surface charges of the localized dipolar plasmon mode on the nanoparticle and the propagating mode at the metal surface²³. As demonstrated in previous experimental and theoretical work, the vertical gap mode presents much stronger nanoparticle-film interaction, resulting in a red-shift of the resonant peak position with respect to the lateral one^{23–26}. This is confirmed with our numerical modeling using the finite difference time domain method, as shown in Fig. 1c, which shows wavelength-dependent averaged Raman enhancement (corresponding to the near-field enhancements, see Methods) within the junction for the two types of gap modes. Thus, at an incident wavelength longer than the intersection wavelength, the near-field enhancement associated with the vertical gap mode is significantly higher than the lateral mode. The enhanced electric field can then be used to boost the

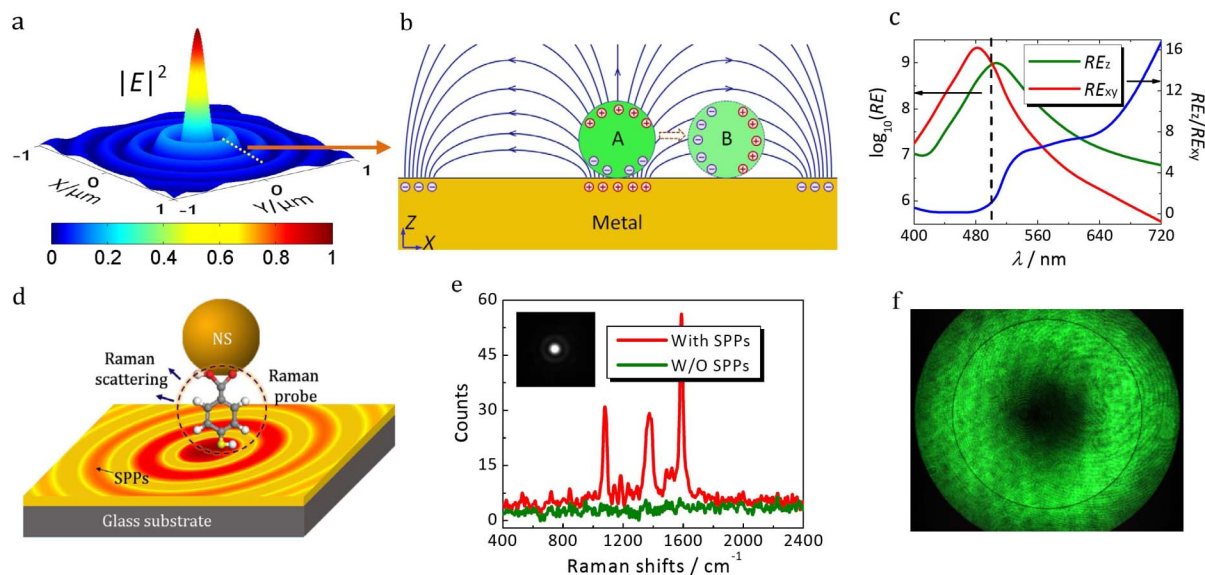


Figure 1 | Concept of plasmon-hybridization directed characterization of surface plasmon perpendicular fields. (a) Spatial distribution of near-fields associated with a typical surface plasmon standing-wave produced by a radially polarized cylindrical beam. (b) Illustration of a nanosphere-film junction coupling to the perpendicular (A) and in-plane (B) electric fields of the standing-wave along the dashed line in (a), resulting in vertical and lateral gap modes, respectively. (c) Calculated averaged Raman enhancement (RE) within the nanosphere-film junction generated by perpendicular (RE_z) and in-plane (RE_{xy}) electric fields of SPPs, exhibiting mode splitting. The blue line illustrates their enhancement ratio. (d) Schematic diagram of the proposed surface plasmon detection system based on plasmonic gap mode-assisted SERS imaging. (e) SERS spectra of 4-MBA molecules collected from a single nanosphere-film junction, with and without SPP excitation. Inset shows a simultaneously-obtained Raman image of a single nanosphere-film junction. (f) Back Fourier plane image of the reflected radially polarized laser beam. The dark ring confirms SPP excitation at the silver-air interface over all azimuthal directions.



SERS intensity of molecules adsorbed within the particle-film gap. Therefore, by exciting the system with a proper wavelength and acquiring the SERS signals through the surface, one can map out indirectly the field-strength of the perpendicular component (Fig. 1d). That is, the nanoparticle-film junction acts as an SPP-antenna, transferring the evanescent surface waves into propagating Raman radiation, with the capability to differentiate plasmon-hybridized gap modes by their different optical responses.

We first examine the near-field distribution of SPPs excited by a tightly focused beam at a wavelength of 532 nm, under an attenuated total reflection configuration with a high numerical aperture objective lens²⁷ (supplementary Fig. S2). To create the nanoparticle-film junctions, a sub-monolayer of 60-nm-diameter silver nanospheres was immobilized on the silver film surface by thiol pairs of 4-mercaptobenzoic acid (4-MBA) molecules²⁸, which were also employed as the Raman probe of the evanescent surface plasmon fields. We have chosen this type of molecule because of their non-fluorescent nature which avoids the uncertainty induced by fluorescence quenching²⁹. As confirmed by dark-field imaging (supplementary Fig. S4), we precisely control the number density of nanospheres to such a degree that only a single nanosphere is located within the propagation region of SPPs. (For details of sample preparation, see “Methods”).

The SERS spectrum of 4-MBA molecules (red curve in Fig. 1e) is collected from a single nanosphere-film junction under radially polarized beam excitation; the inset shows the Raman image captured by a CCD camera at the position of maximum Raman intensity. The SPP excitation is confirmed with the reflected laser beam obtained at the back Fourier plane (See Fig. 1f) of the objective lens. A dark ring is clearly seen in the reflection beam, meaning a reflectivity dip in the reflection spectrum, and thus indicating the excitation of SPPs at the silver-air interface. We then reduced the incident beam size gradually with an adjustable iris aperture placed just beneath the objective lens. The intensity and spectrum of the SERS signal did not show significant changes until the dark ring has

just disappeared. Under this circumstance, the Raman image of the nanoparticle-film junction cannot be seen by the CCD camera; the corresponding SERS spectrum, the green curve in Fig. 1e, shows only dark noise. This is evidence that the collected SERS signal from molecules is mainly enhanced by evanescent surface plasmon fields, rather than by directly transmitted light or evanescent waves induced by total internal reflection at incident angles larger than the excitation angle of the SPP resonance. Such complete suppression of Raman excitations from transmitted light confirms the correlation between the SERS imaging and the near-field spatial profile of SPPs.

Mapping surface plasmon fields by SERS imaging. The spatial mapping of surface plasmon standing-waves, presented in Fig. 2, were obtained by raster scanning the nanoparticle-film junction over the propagation region of SPPs and recording the intensity of SERS at each point (supplementary movie). A radially polarized cylindrical beam was employed to excite the SPPs in Fig. 2a. Because of the *p*-polarization state inside the full beam, SPPs can be excited along all azimuthal directions, forming a sub-diffraction-limited evanescent plasmon spot at its center (Fig. 2(a1)). This measured pattern is in excellent agreement with the calculated perpendicular field component (Fig. 2(a2)), but juxtaposes the in-plane field distribution (Fig. 2(a3)), a typical near-field pattern obtained by aperture-type SNOM measurements. The agreement can be assessed quantitatively by plotting their intensity curves across the center as we will discuss later. All the theoretical calculations are carried out within the framework of the Richard-Wolf vectorial diffraction method³⁰ for a bare Ag film without the presence of Ag nanosphere. As apparent, for excitations of plasmon gap modes with a dominant perpendicular field component of the electric field, the presence of the nanosphere in experimental samples induces only a small perturbation to the distribution of SPP fields on the metal film.

Figure 2(b1–3) present spatial mappings of surface plasmon fields generated under other frequently-used polarized-beams, including a

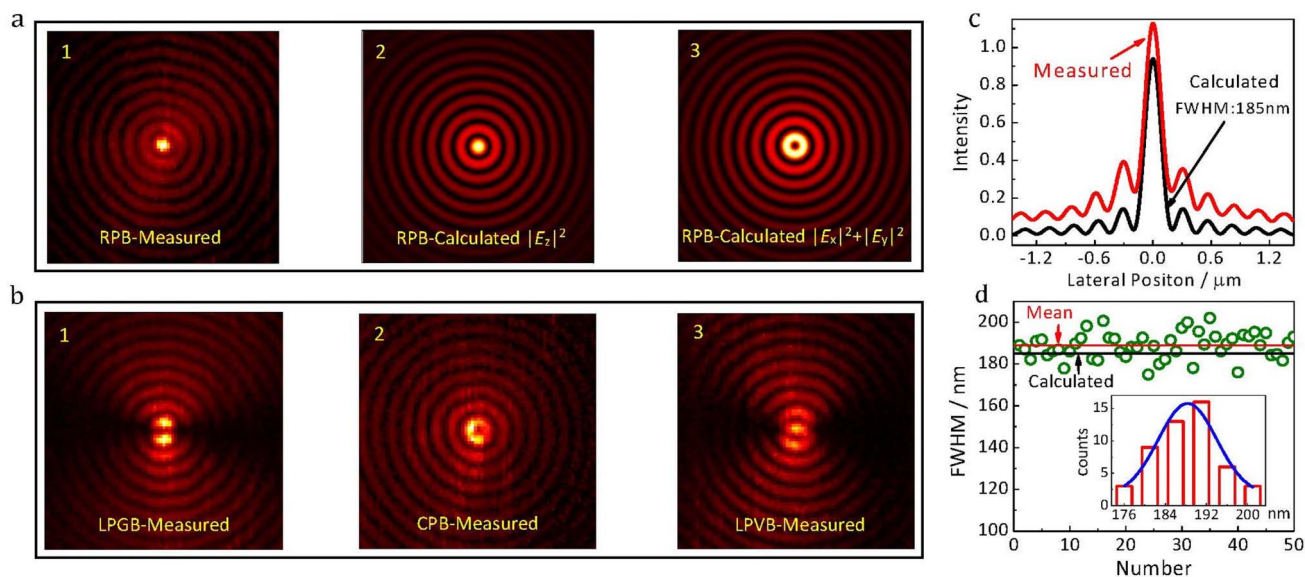


Figure 2 | Mapping surface plasmon standing-waves with gap mode SERS imaging. (a) Measured plasmonic near-field distribution produced by a tightly-focused radially polarized beam (RPB) (a1), compared with the calculated perpendicular (a2) and in-plane (a3) electric field components. (b) The corresponding mappings of surface plasmon fields generated under a tightly-focused linearly polarized Gaussian beam (LPG) (b1), a circularly polarized beam (CPB) (b2) and a linearly polarized optical-vortex beam (LPVB) of charge “1” (b3), to verify further the perpendicular field sensitivity of our method and the RPB capability to produce a strongly confined perpendicular field at the center. (c) Cross-section comparison between measured plasmon field (a1) and calculated perpendicular field component (a2). (d) Statistical measurement of the lateral field-extension of the central spot with 50 randomly-selected nanospheres on the metal film, verifying accuracy and reproducibility of our measurement. Incident wavelength is 532 nm in all cases. Area of each contour map is $4 \mu\text{m} \times 4 \mu\text{m}$.



tightly-focused linearly polarized Gaussian beam, a circularly polarized beam, and a linearly polarized optical-vortex beam of charge “1”³³. All the measured results are in good agreement with calculated perpendicular field distributions (supplementary Fig. S3). These results not only illustrate clearly that the plasmonic near-field distribution recorded by SERS imaging is sensitive to the perpendicular SPP field for which a bright or dark central spot is highly polarization-dependent, but also reveal explicitly the capability of a radially polarized beam to form a strongly-confined perpendicular field because of its full-beam *p*-polarization and in-phase plasmon excitation. This capability is missed in other beams either because of the spatially-variant *p*-polarization in Fig. 2(b1) and 2(b3) or because of the out-of-phase excitation of SPPs in Fig. 2(b1) and 2(b2).

As mentioned above, the lateral extension of the strongly-confined perpendicular field can be extracted through plotting the Raman intensity across the center of a standing-wave. Figure 2c shows a comparison between the experimental result extracted from Fig. 2(a1) and our calculation result based on the Richard-Wolf method. By measuring the full width at half maximum (FWHM) of the central peak, we can obtain the lateral field extension. The results from 50 randomly-selected silver nanospheres are presented in Fig. 2d, showing measured spot sizes approximately following a normal distribution (see inset) with mean value of 189 nm ($0.355\lambda_0$) and standard deviation of 7 nm. The slight deviation from the theoretical value (185 nm) could be attributed to the difference in the electric permittivity for the silver film used in our experiment and that used in the numerical calculations and to the perturbation of the presence of the nanoparticle on SPPs as well as the finite scanning step size of 40 nm. The excellent agreement of mean value and small standard deviation indicate a high reproducibility as well as the high accuracy of our measurements. To the best of our knowledge, this is the first direct measurement of the spot size of a plasmon virtual probe down to the sub-wavelength scale in the visible range.

Unveiling nano-focusing interferences of plasmon lens systems.

Plasmon lenses are the near-field counterpart of conventional optical lenses, with which surface plasmon fields can be focused to form a spot with tuned-dimensions^{32,33}. Their integration with

plasmon waveguides offers great potential in applications such as miniaturized photonic circuits. Thus, it is particularly important to uncover the near-field behavior of a specific plasmon lens before using it in practical applications. Here we apply the developed SERS imaging method to study the focusing process of surface plasmon waves created by arc-shaped structure-free plasmon lenses (Figs. 3 and 4). Such plasmon lenses are achieved by a tightly-focused radially polarized cylindrical beam but with only a single (Fig. 3a) or few arc-shaped beam segments (Fig. 4a and b) for SPPs excitation, exhibiting their directional, dynamic and reconfigurable advantages. (For details of the structure-free plasmon lenses, see supplementary Fig. S2)

The experimentally-measured Raman intensity distributions and the theoretically-calculated near-field profiles (Fig. 3b–d) were compared for plasmon lenses of various expanding angles. The dimensions of the focal spot can effectively be tuned by changing the expanding angle; the larger the angle, the more confined the spot. This is similar in concept to the numerical aperture of an optical lens, which is defined as $n \times \sin(\theta/2)$, where n represents the refractive index of the medium and θ the expanding angle of the lens. For the purpose of comparison, we calculated the corresponding near-field distributions using the Richard-Wolf method, with the results shown in the right column of Fig. 3b–d (red-white contour maps). The exact details of the interference fringes are clearly visualized, matching experimental observations.

As a final demonstration, we investigate the near-field interference process of SPPs in systems consisting of multiple plasmon lenses. For simplicity, we consider only symmetrically arranged quadruple- and triple-arcs, schematically illustrated in Fig. 4a and b, respectively. The expanding angle for each plasmon lens in the calculation and experiment is set at 30° . The calculated plasmon fields, shown in Fig. 4c and d, both present a set of plasmonic focal spots within the central area but with different arrangements. The quadruple lens system formed a face-centered arrangement whereas the triple lens formed a close-packed hexagonal arrangement. Again, the measured interference patterns within the central area (see Fig. 4e) through SERS imaging unambiguously reveal complex near-field interferences of each lens system. By carefully designing the number,

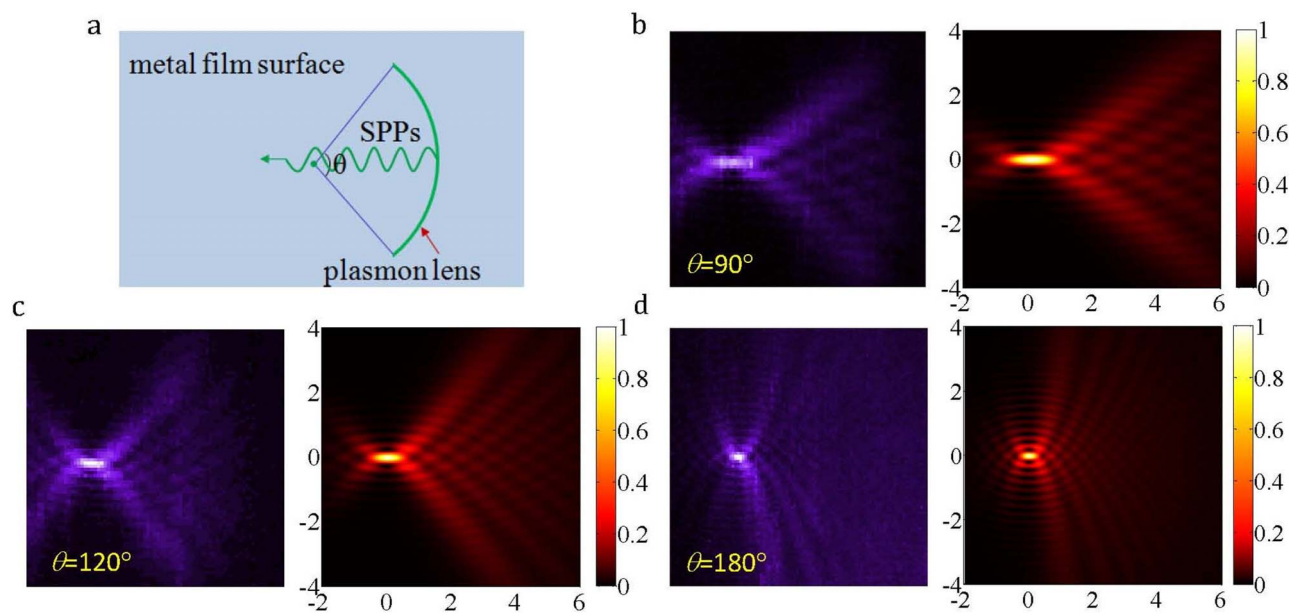


Figure 3 | Uncovering the near-field dynamics of an arc-shaped structure-free plasmon lens. (a) Schematic illustration of the lens produced from focusing an arc-shaped RPB segment defined by expanding angle θ . SPPs from the lens propagate radially towards the center, forming a plasmonic focal spot. (b)–(d) Experimentally measured (purple-white) and calculated (red-white) plasmon fields at the metal surface under expanding angles 90° , 120° , and 180° , respectively, showing strong matches. Area of each contour map is $8 \mu\text{m} \times 8 \mu\text{m}$.

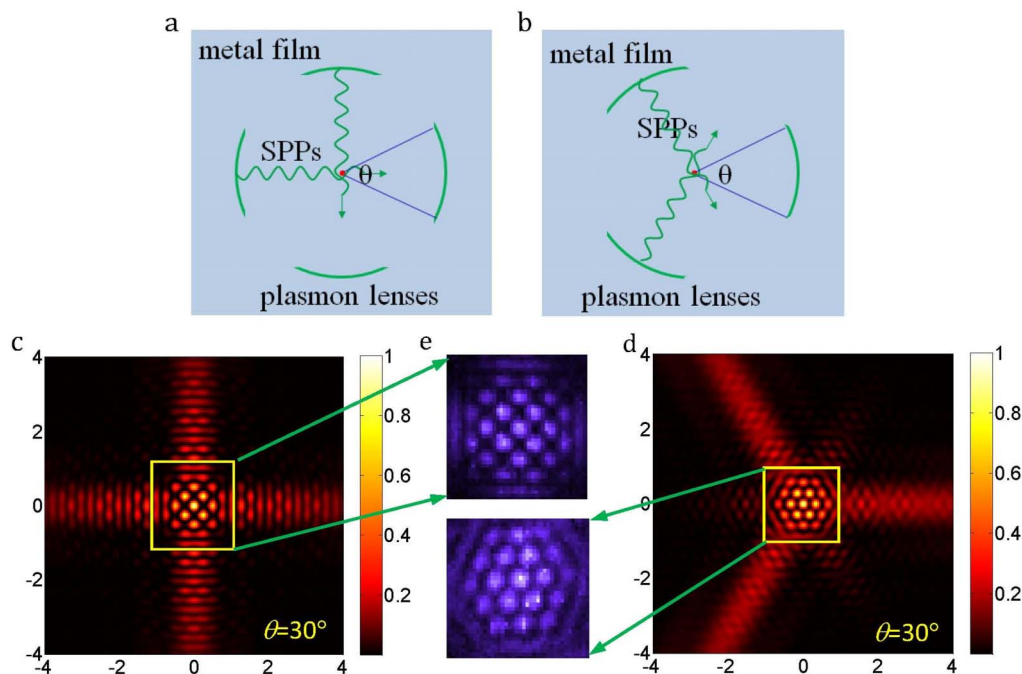


Figure 4 | Revealing the interference process of multiple-plasmon-lens systems. (a) and (b) Schematic illustration of symmetrically arranged quadruple- and triple-plasmon-lens systems. (c) and (d) Calculated plasmon fields using vectorial diffraction method under 30° expanding angle. (e) Measured interference patterns in the central area with SERS imaging, for quadruple-plasmon lens (upper panel) and triple-plasmon lens (lower panel). The near-field behavior of the plasmon dynamics is well revealed. Area of each calculated contour map is $8 \mu\text{m} \times 8 \mu\text{m}$.

arrangement, and expanding angle of plasmon lenses, a variety of interference patterns can be created, which can be used for applications such as nanolithography.

Discussion

Above, we have demonstrated a variant scheme of scattering-type SNOM to map near-field interferences of SPPs with high spatial resolution. On the one hand, a nanoparticle-film junction, instead of a motorized metallic tip, is employed as a surface plasmon antenna, which not only simplifies greatly the detection configuration, but also preserves the perpendicular field sensitivity because of the polarization-resolved excitation of plasmon-hybridized gap modes. This is particularly important for a complete characterization of SPPs fields because the perpendicular field component usually dominates over the total field strength for SPPs of wave vectors close to the light line. In general, a gap distance below 5 nm is sufficient to induce strong coupling between the nanoparticle and the film and the subsequent Raman mapping. A larger gap distance (>10 nm, for example) results in weak coupling between the nanoparticle and film and thus a weak near-field enhancement that is not sufficient to enhance the Raman intensity from the molecules in between.

In our scheme, on the other hand, surface-enhanced Raman scattering instead of Rayleigh scattering is collected for SPPs characterization. Although Rayleigh scattering possesses a larger scattering cross-section, its wavelength is exactly the same as the illuminating wavelength and hence is hard to extract from the incident light. Raman scattering, in contrast, shows a small wavelength shift with respect to the initial illumination, thus easily extracted using a notch (or long-pass) filter. Meanwhile, because of the excitation of the plasmon-hybridized gap mode, Raman scattering can be significantly enhanced by more than 10^8 for a nanoparticle-film junction excitation scheme. This greatly compensates for the small normal Raman scattering cross-section and hence improves the signal-to-noise ratio.

Finally, using the SERS imaging improves resolution, which is determined by the gap-mode volume within the nanoparticle-film

junction. By reducing the nanoparticle size, resolutions of less than 50 nm can easily be achieved. The nanoparticle size between 40–100 nm is appropriate for our experiment since their localized surface plasmon resonant wavelengths locate at the visible range covering the laser excitation wavelength. If the nanoparticle is too large, it will not only induce a large perturbation on SPPs, but also impair the resolution of our method. If it is too small, its resonant wavelength is away from the incident wavelength, leading to a weak Raman enhancement and a low signal to noise ratio.

We believe that the SERS imaging can serve as a generic SPP detection tool. When working together with the conventional SNOM system, it will provide a deeper and more complete understanding of near-field interferences of these versatile SPPs, and will be very helpful in a broad range of applications such as miniaturized photonic circuits, nanolithography, and super-resolution imaging.

Methods

Sample preparation. 4-MBA molecules and silver colloidal nanosphere solution (nominal diameter ~ 60 nm, 10^{10} nanospheres per mL) were purchased from Sigma-Aldrich and nanoComposix, respectively. Silver film with thickness of 45 nm was deposited by electron beam deposition on a cleaned glass coverslip. The coated substrate was then immersed for around 10 mins in a 10^{-3} M ethanolic 4-MBA solution to form a self-assembled monolayer (SAM) of 4-MBA molecules. The sample was subsequently rinsed with ethanol and DI water to remove excess molecules on the surface. Finally, a droplet of diluted Ag colloids (100 μL , $\sim 10^9$ nanospheres per mL) was deposited onto the SAM/Ag plane and allowed to evaporate naturally, followed by water-rinsing and air-drying at ambient temperature.

Generation of radially polarized light and linearly polarized vortex beam. Radially polarized beam is converted from a circularly polarized beam by passing it through a spiral phase element (to compensate for the geometric phase of circular polarization), an azimuthal-type analyzer (to filter out the radial component) and two half waveplates angled with 45° (to rotate the azimuthal polarization into the radial polarization), respectively. Vortex beam is achieved simply by illuminating a linearly polarized Gaussian beam onto a spatial light modulator, which generates the required spiral phase of a vortex beam.

Experimental apparatus. An Olympus oil immersion objective lens ($60\times$, $\text{NA} = 1.49$) was used to focus the collimated incident beams on to the silver-air interface to excite the SPPs. Raman images of immobilized Ag nanospheres on Ag film were captured with a Thorlabs digital CCD camera. Meanwhile, Raman signals emitted



from 4-MBA molecules located at the nanosphere-film junction were obtained with an OceanOptics TEC cooling spectrometer (QE65000). A piezo-scanning stage (Physikinstrumente (PI), P545.3R7) was used initially to position the nanosphere at the center of focal plane, by monitoring the intensity of Raman signal collected by the spectrometer and the CCD camera, and subsequently to raster scan the nanosphere over the SPP region to get the SPP near-field distribution.

SPP characterization. After an isolated nanosphere was found (checked with the CCD camera) and positioned at the center of focal plane, Raman signals emitted from 4-MBA molecules were sent for further amplification to a Hamamatsu photomultiplier tube (PMT), instead of the spectrometer. The scanning of PI stage, the acquisition of data from the PMT, and the real-time displaying of SPP distribution were all realized and coordinated via LabView software. For the two-dimensional mapping of the SPP standing-waves, scanning range and step size were set to $5 \mu\text{m} \times 5 \mu\text{m}$ and 50 nm respectively; for the spot-size measurement of plasmon virtual probe, the scanning range in the X direction was set to 400 nm to trace the cross-section distribution across the center, and that for the Y direction was set to $4 \mu\text{m}$ for the actual measurements. The step size for both directions was set to 40 nm . For the mapping of the nano-focusing of SPPs, the scanning range is $8 \mu\text{m} \times 8 \mu\text{m}$ with scanning step of 100 nm .

Raman enhancement calculation. The averaged Raman enhancement within the junction is employed to evaluate the field sensitivity of a nanoparticle-film junction, which is calculated using:

$$RE_p = \left(\frac{\sum_{ij} \frac{|E_{ij}^{loc}|^4}{|E_{ij}^{SPP}|^4} |E_{ij}^{SPP}|^2}{|E_p^{SPP}|^2} \right)^2$$

in which E_{ij}^{loc} denotes the amplitude of the enhanced electric field localized within the junction at the horizontal gap plane, E_{ij}^{SPP} the SPP amplitude above the metal film in the absence of a nanosphere, and p (either “z” or “xy”) represents the polarization of surface plasmon fields (perpendicular or in-plane field, corresponding to the vertical or lateral gap mode), respectively. Vertical and lateral gap modes are produced by sitting the nanosphere on the standing-wave node and anti-node of the SPPs, (see Fig. 1b).

- Barnes, W. L., Dereux, A. & Ebbesen, T. W. Surface plasmon subwavelength optics. *Nature* **424**, 824–830 (2003).
- Schmidt, M. A., Lei, D. Y., Wondraczek, L., Nazabal, V. & Maier, S. A. Hybrid nanoparticle-microcavity-based plasmonic nanosensors with improved detection resolution and extended remote-sensing ability. *Nat. Commun.* **3**, 1108 (2012).
- Homola, J., Yee, S. S. & Gauglitz, G. Surface plasmon resonance sensors: Review. *Sens. Actuat. B-Chem.* **54**, 3–15 (1999).
- Pendry, J. B. Negative refraction makes a perfect lens. *Phys. Rev. Lett.* **85**, 3966–3969 (2000).
- Fang, N., Lee, H., Sun, C. & Zhang, X. Sub-diffraction-limited optical imaging with a silver superlens. *Science* **308**, 534–537 (2005).
- Pendry, J. Playing tricks with light. *Science* **285**, 1687–1688 (1999).
- Novotny, L. & Stranick, S. J. *Annu. Rev. Phys. Chem.* **57**, 303–331 (2006).
- Weeber, J. C. *et al.* Near-field observation of surface plasmon polariton propagation on thin metal stripes. *Phys. Rev. B* **64** (2001).
- Liu, Z. W. *et al.* Focusing surface plasmons with a plasmonic lens. *Nano. Lett.* **5**, 1726–1729 (2005).
- Bouhelier, A. *et al.* Surface plasmon interference excited by tightly focused laser beams. *Opt. Lett.* **32**, 2535–2537 (2007).
- Zia, R. & Brongersma, M. L. Surface plasmon polariton analogue to young’s double-slit experiment. *Nat. Nanotechnol.* **2**, 426–429 (2007).
- Chen, W. B., Aboesinghe, D. C., Nelson, R. L. & Zhan, Q. W. Plasmonic lens made of multiple concentric metallic rings under radially polarized illumination. *Nano. Lett.* **9**, 4320–4325 (2009).
- Tan, P. S. *et al.* Phase singularity of surface plasmon polaritons generated by optical vortices. *Opt. Lett.* **36**, 3287–3289 (2011).
- Vanlabekke, D. & Barchiesi, D. Probes for scanning tunneling optical microscopy - a theoretical comparison. *J. Opt. Soc. Am. A* **10**, 2193–2201 (1993).
- Zayats, A. V., Smolyaninov, I. I. & Maradudin, A. A. Nano-optics of surface plasmon polaritons. *Phys. Rep.* **408**, 131–314 (2005).
- Lerman, G. M., Yanai, A. & Levy, U. Demonstration of nanofocusing by the use of plasmonic lens illuminated with radially polarized light. *Nano. Lett.* **9**, 2139–2143 (2009).
- Chen, J. N. *et al.* Optical nano-imaging of gate-tunable graphene plasmons. *Nature* **487**, 77–81 (2012).
- Fei, Z. *et al.* Gate-tuning of graphene plasmons revealed by infrared nano-imaging. *Nature* **487**, 82–85 (2012).
- Ogawa, Y., Takahashi, S., Nakajima, D. & Minami, F. Imaging of surface plasmon polariton propagation on a Au thin film by using tip-enhanced Rayleigh scattering. *J. Lumin.* **133**, 145–148 (2013).
- Drezet, A. *et al.* Leakage radiation microscopy of surface plasmon polaritons. *Mater. Sci. Eng., B* **149**, 220–229 (2008).
- Ditlbacher, H. *et al.* Fluorescence imaging of surface plasmon fields. *Appl. Phys. Lett.* **80**, 404–406 (2002).
- Moh, K. J., Yuan, X. C., Bu, J., Zhu, S. W. & Gao, B. Z. Surface plasmon resonance imaging of cell-substrate contacts with radially polarized beams. *Opt. Express* **16**, 20734–20741 (2008).
- Nordlander, P. & Prodan, E. Plasmon hybridization in nanoparticles near metallic surfaces. *Nano. Lett.* **4**, 2209–2213 (2004).
- Mock, J. J. *et al.* Distance-dependent plasmon resonant coupling between a gold nanoparticle and gold film. *Nano. Lett.* **8**, 2245–2252 (2008).
- Yamamoto, N., Ohtani, S. & de Abajo, F. J. G. Gap and mie plasmons in individual silver nanospheres near a silver surface. *Nano. Lett.* **11**, 91–95 (2011).
- Lei, D. Y. *et al.* Revealing plasmonic gap modes in particle-on-film systems using dark-field spectroscopy. *ACS Nano* **6**, 1380–1386 (2012).
- Du, L. P., Yuan, G. H., Tang, D. Y. & Yuan, X. C. Tightly focused radially polarized beam for propagating surface plasmon-assisted gap-mode Raman spectroscopy. *Plasmonics* **6**, 651–657 (2011).
- Orendorff, C. J., Gole, A., Sau, T. K. & Murphy, C. J. Surface-enhanced Raman spectroscopy of self-assembled monolayers: Sandwich architecture and nanoparticle shape dependence. *Anal. Chem.* **77**, 3261–3266 (2005).
- Dulkeith, E. *et al.* Fluorescence quenching of dye molecules near gold nanoparticles: Radiative and nonradiative effects. *Phys. Rev. Lett.* **89**, 203002 (2002).
- Youngworth, K. S. & Brown, T. G. Focusing of high numerical aperture cylindrical-vector beams. *Opt. Express* **7**, 77–87 (2000).
- Tan, P. S., Yuan, X. C., Lin, J., Wang, Q. & Burge, R. E. Analysis of surface plasmon interference pattern formed by optical vortex beams. *Opt. Express* **16**, 18451–18456 (2008).
- Yin, L. L. *et al.* Subwavelength focusing and guiding of surface plasmons. *Nano. Lett.* **5**, 1399–1402 (2005).
- Imre, A., Vlasko-Vlasov, V. K., Pearson, J., Hiller, J. M. & Welp, U. Multiplexing surface plasmon polaritons on nanowires. *Appl. Phys. Lett.* **91** (2007).

Acknowledgements

This work was partially supported by the National Natural Science Foundation of China under Grant Nos. (61036013, 61138003), Ministry of Science and Technology of China under Grant No. 2009DFA52300 for China-Singapore collaborations, and National Research Foundation of Singapore under Grant No. NRF-G-CRP 2007-01. S.A.M. acknowledges the financial support by the Engineering and Physical Sciences Council of the United Kingdom and Leverhulme Trust. D.Y.L. acknowledges the grants 1-ZVAL and 1-ZVAW administered by the Hong Kong Polytechnic University. X.C.Y. acknowledges the support given by Tianjin Municipal Science and Technology Commission under Grant No. 11JCZDJ15200.

Author contributions

L.D. and X.Y. jointly conceived the idea of this study. L.D. designed and carried out the experiment, performed the simulation and prepared the manuscript. G.Y. and X.Z. assisted in the numerical and theoretical analysis. D.Y.L., H.F., Q.W., D.T., C.M., S.A.M. and X.Y. helped analyze the results and prepare the manuscript. X.Y. supervised and coordinated all of the work. All of the authors discussed the results and manuscript extensively.

Additional information

Supplementary information accompanies this paper at <http://www.nature.com/scientificreports>

Competing financial interests: The authors declare no competing financial interests.

How to cite this article: Du, L. *et al.* Mapping plasmonic near-field profiles and interferences by surface-enhanced Raman scattering. *Sci. Rep.* **3**, 3064; DOI:10.1038/srep03064 (2013).



This work is licensed under a Creative Commons Attribution-NonCommercial-NoDerivs 3.0 Unported license. To view a copy of this license, visit <http://creativecommons.org/licenses/by-nc-nd/3.0>